

3-2018

# Development of a semigraphitic sulfur-doped ordered mesoporous carbon material for electroanalytical applications

Jaqueline R. Maluta  
*University of São Paulo*

Sergio A.S. Machado  
*University of São Paulo*

Umesh Chaudhary  
*Iowa State University and Ames Laboratory*

J. Sebastian Manzano  
*Iowa State University and Ames Laboratory, smanzano@iastate.edu*

Lauro T. Kubota  
*Institute of Chemistry – UNICAMP*

*See next page for additional authors*

Follow this and additional works at: [http://lib.dr.iastate.edu/ameslab\\_manuscripts](http://lib.dr.iastate.edu/ameslab_manuscripts)

 Part of the [Materials Chemistry Commons](#), [Nanoscience and Nanotechnology Commons](#), and the [Physical Chemistry Commons](#)

---

## Recommended Citation

Maluta, Jaqueline R.; Machado, Sergio A.S.; Chaudhary, Umesh; Manzano, J. Sebastian; Kubota, Lauro T.; and Slowing, Igor I., "Development of a semigraphitic sulfur-doped ordered mesoporous carbon material for electroanalytical applications" (2018). *Ames Laboratory Accepted Manuscripts*. 69.  
[http://lib.dr.iastate.edu/ameslab\\_manuscripts/69](http://lib.dr.iastate.edu/ameslab_manuscripts/69)

This Article is brought to you for free and open access by the Ames Laboratory at Iowa State University Digital Repository. It has been accepted for inclusion in Ames Laboratory Accepted Manuscripts by an authorized administrator of Iowa State University Digital Repository. For more information, please contact [digirep@iastate.edu](mailto:digirep@iastate.edu).

---

# Development of a semigraphitic sulfur-doped ordered mesoporous carbon material for electroanalytical applications

## Abstract

The modification of traditional electrodes with mesoporous carbons is a promising strategy to produce high performance electrodes for electrochemical sensing. The high surface area of mesoporous carbons provides a large number of electroactive sites for binding analytes. Controlling the pore size and structure of mesoporous carbons and modifying their electronic properties via doping offers additional benefits like maximizing transport and tuning the electrochemical processes associated with analyte detection. This work reports a facile method to produce sulfur-doped ordered mesoporous carbon materials (S-OMC) with uniform pore structure, large pore volume, high surface area and semigraphitic structure. The synthesis used thiophenol as a single source of carbon and sulfur, and iron as a catalyst for low temperature carbonization. The S-OMC material was deposited on a glassy carbon electrode and used as a sensor with high sensitivity ( $11.7 \text{ A L mol}^{-1}$ ) and selectivity for chloramphenicol detection in presence of other antibiotics. As a proof-of-concept, the sensor was applied to the direct analysis of the drug in reconstituted powdered milk and in commercial eye drops.

## Keywords

Ordered mesoporous carbon, Sulfur-doped carbon, Mesoporous silica nanoparticles, Electrochemical sensor, Chloramphenicol detection

## Disciplines

Materials Chemistry | Nanoscience and Nanotechnology | Physical Chemistry

## Authors

Jaqueline R. Maluta, Sergio A.S. Machado, Umesh Chaudhary, J. Sebastian Manzano, Lauro T. Kubota, and Igor I. Slowing



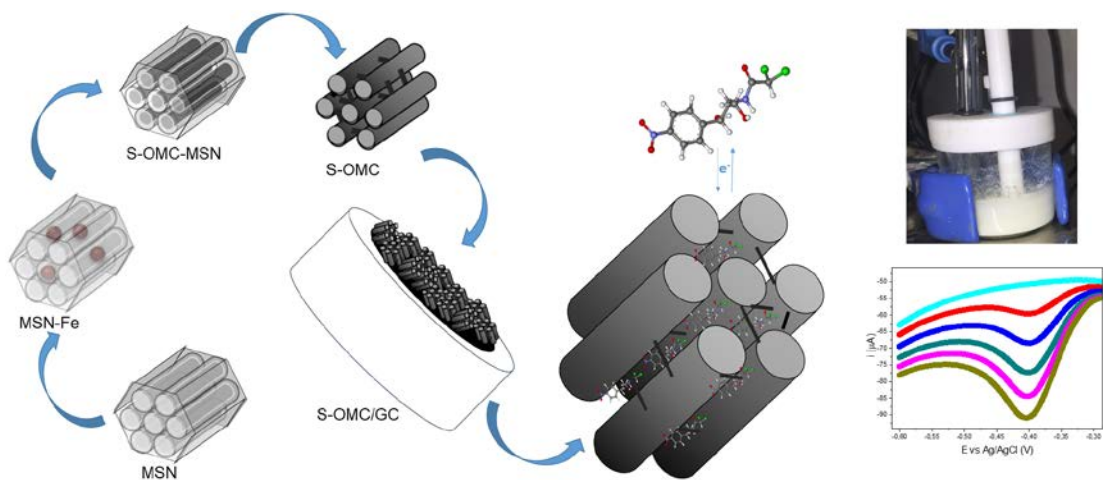
24 **Highlights**

25

- 26 • Thiophenol as a new source to produce S-doped ordered mesoporous carbons (S-  
27 OMC).
- 28 • Iron in silica template catalyzes low temperature carbonization in S-OMC synthesis.
- 29 • Fast electron transfer and conductivity make S-OMC suitable to produce electrodes.
- 30 • S-OMC modified GC electrodes display ppb sensitivity for selective CAP detection.
- 31 • S-OMC/GC electrodes quantify CAP in powdered milk without any sample  
32 preparation.

33

34 **Graphical abstract**



35

36

37 **Abstract**

38 A promising strategy to produce high performance electrodes for electrochemical sensing is  
39 the modification of traditional electrodes with mesoporous carbons. The high surface area  
40 of these materials provides a large number of electroactive sites for binding analytes.  
41 Controlling the pore size and structure of mesoporous carbons and modifying their  
42 electronic properties via doping offers additional benefits like maximizing transport and  
43 tuning the electrochemical processes associated with analyte detection. This work reports a  
44 facile method to produce sulfur-doped ordered mesoporous carbon materials (S-OMC) with  
45 uniform pore structure, large pore volume, high surface area and semigraphitic structure.  
46 The synthesis uses thiophenol as the single source of carbon and sulfur, and iron as catalyst  
47 for low temperature carbonization. The S-OMC material was assembled on a glassy carbon  
48 electrode and used as a sensor with excellent sensitivity ( $18.9 \text{ A} \cdot \text{L} \cdot \text{mol}^{-1}$ ) and selectivity  
49 for chloramphenicol detection in presence of other antibiotics. The sensor was successfully  
50 used for direct analysis of the drug in milk without requiring any sample preparation.

51

52

53

54

55

56

57

58

59

60

61 **Keywords:** ordered mesoporous carbon, sulfur-doped carbon, mesoporous silica  
62 nanoparticles, electrochemical sensor, chloramphenicol detection

63

## 64 **1. Introduction**

65 Several different carbon materials are used in electroanalysis due to their electrical  
66 conductivity, chemical inertness, and low background current.[1] Nanostructured carbons  
67 such as ordered mesoporous carbons (OMC) have the additional benefits of uniform pore  
68 structures, large pore volumes, high specific surface areas, and tunable pore size  
69 distributions, which can maximize the interaction with analytes and ensure fast mass  
70 transport.[2, 3] Furthermore, due to their fast electron transfer capacity and excellent  
71 electrocatalytic activity, OMC have been recently used in sensing,[4] with excellent  
72 performance in detection of morphine, epinephrine, acetaminophen, H<sub>2</sub>O<sub>2</sub>, nitrobenzene,  
73 and NADH.[5-7] The superb electrochemical behavior of OMC may be attributed to a large  
74 number of edge plane defect sites on their accessible surface.[6]

75 OMC are typically synthesized by infiltration of the pores of a mesoporous silica  
76 template with appropriate carbon precursor, followed by carbonization, and subsequent  
77 template removal.[8] The graphitic character of OMC determines its electrical conductivity,  
78 and is key for its electrochemical applications.[9] A high graphitic character and electrical  
79 conductivity can be achieved by using aromatic precursors,[10] carbonizing at high  
80 pressures,[11] chemical vapor deposition,[12] or addition of iron as carbonization  
81 catalyst.[13, 14]

82 The electronic properties of OMC can be controlled by incorporating heteroatoms  
83 into their structure. While nitrogen doping of OMC has been widely explored,[15] sulfur  
84 doping is less common. S-doped OMC (S-OMC) have been obtained by post-synthesis  
85 treatment using melt-diffusion,[16-18] or directly synthesized using sulfur-containing  
86 molecules like p-toluenesulfonic acid or benzyl disulfide as carbon source.[19-21] These S-  
87 doped materials have been used to promote metal-support interactions in the catalytic  
88 oxygen reduction reaction,[21] and in the adsorption of acetaminophen,[22, 23]  
89 oxygen,[24, 25] and dibenzothiophene.[26, 27]

90 Chloramphenicol (CAP) is a broad-spectrum antimicrobial with remarkable  
91 antibacterial and pharmacokinetic properties. However, this drug is considered an  
92 environmental contaminant and is forbidden for use in food-producing animals[28, 29]  
93 because it is associated with human health issues such as aplastic anemia, hepatic  
94 dysfunction, gray syndrome, and cancer.[30, 31] In spite of this status, the Rapid Alert

95 System for Food and Feed (RASFF) of the European Union has reported over 80  
96 notifications of the illegal use of CAP between 2010 and 2017.[32] Therefore, the detection  
97 of this drug has financial, environmental, and public health importance. Herein, we report  
98 the synthesis and characterization of an S-OMC with semi-graphitic character prepared  
99 using thiophenol as an aromatic S-containing carbon precursor and iron as a catalyst.  
100 Because of its adsorptive and electrochemical properties, the material was used to assemble  
101 modified electrodes for the direct detection and quantification of ppb levels of CAP.

102

## 103 **2. Materials and methods**

### 104 *2.1 Preparation of S-OMC*

105 SBA-15 type mesoporous silica nanoparticles (MSN) were synthesized following  
106 previous reports.[33] Briefly, 7.0 g of Pluronic P-104 was dissolved in 164 mL of Millipore  
107 water and 109 mL of HCl 4.0 M. The resulting solution was stirred for 1 h at 52 °C. Then,  
108 10.64 g of TMOS was added and the solution was stirred for further 24 h at 52 °C. After  
109 this, the solution was placed in an autoclave for hydrothermal treatment at 150 °C for  
110 additional 24 h. The MSN product was then filtered, washed with ethanol and dried in air.  
111 The surfactant was removed by calcination in air at 550 °C for 6 h. Following a literature  
112 procedure, [3, 10] a solution of  $\text{Fe}(\text{NO}_3)_3 \cdot 9\text{H}_2\text{O}$  (0.382 g, 0.764 g, or 1.145 g) in acetone (1  
113 mL) was impregnated into the MSN (1.0 g), and calcined in air at 350 °C for 6 h. Finally,  
114 the ordered mesoporous carbon (OMC) was synthesized by impregnating 1.0 g of Fe-MSN  
115 composite with 9 mmol of thiophenol, drying at 70 °C and carbonizing at 600 °C or 900 °C  
116 during 7 h under flowing Ar. The silica template was removed by refluxing in a  
117 water:ethanol (1:1) solution of NaOH (1 M) overnight at 80 °C (twice). The resulting S-  
118 OMC material was filtered out, washed with Millipore water and dried in air at 70 °C.

119

### 120 *2.2 Characterization*

121 Wide and low angle X-ray diffraction (XRD) patterns were acquired using a  
122 Shimadzu XRR7000 and a BRUKER APEX II Duo, respectively. Both diffractometers  
123 used  $\text{Cu K}\alpha$  ( $\lambda=1.5405\text{\AA}$ ) radiation source operating at 40 kV and 30 mA. Raman spectra  
124 were acquired on a confocal Horiba Scientific T64000 Raman spectrometer using a 633 nm  
125 laser as the excitation source. The powdered materials were directly analyzed by infrared



126 spectroscopy in Attenuated Total Reflectance mode (IR-ATR) using a Bruker Vertex80 FT-  
127 IR spectrometer. The surface area and porosity were measured by nitrogen sorption  
128 isotherms at 196 °C in a Micromeritics TriStar instrument after a 6 h pre-treatment at 100  
129 °C under N<sub>2</sub> flow. The surface area was calculated by Brunauer-Emmett-Teller (BET)  
130 methodology and the pore size distribution by Barret-Joyner-Halenda (BJH). Scanning  
131 electron microscopy was performed with a JEOL JSM634 F equipped with Field Emission  
132 Gun (SEM-FEG). Electron diffraction spectrometry (EDS) was realized at Eletronic  
133 Microscopy ZEISS LEO 440 (Cambridge, England) linked with EDX LINK  
134 ANALYTICAL, (Isis System Series 300) detector. Transmission electron microscopy  
135 (TEM) was performed with LIBRA120 microscope.

136

### 137 *2.3 Electrochemical measurements*

138 The electrochemical measurements were performed in an AUTOLAB PGSTAT 12,  
139 interfaced with NOVA software, using a three-electrode cell. Ag/AgCl (3M KCl) and Pt  
140 foil (1 cm<sup>2</sup>) were used as reference and counter electrode respectively. As working  
141 electrode, a glassy carbon (GC) electrode (3 mm diameter), was polished with alumina and  
142 rinsed thoroughly with doubly distilled water. Then, 10 µL of the respective S-OMC  
143 dispersion (2.0 ± 0.05 mg S-OMC in 1 mL DMF) was drop casted onto the surface of the  
144 GC electrode and dried to obtain an S-OMC/GC modified electrode. The electrolyte was  
145 bubbled with N<sub>2</sub> to remove O<sub>2</sub> before the experiments.

146

## 147 **3. Results and discussion**

### 148 *3.1 S-OMC synthesis*

149 Iron is a well-known carbon polymerization catalyst,[34, 35] therefore it was used  
150 to promote the OMC synthesis (Scheme 1). Impregnation of Fe(NO<sub>3</sub>)<sub>3</sub>•9H<sub>2</sub>O (0.382 g,  
151 0.95 mmol) on SBA-15 type mesoporous silica nanoparticles (MSN) (1.0 g) followed by  
152 calcination led to a small decrease in the surface area and pore volume of the material  
153 (Table 1). SEM imaging of the composite showed no evidence of free iron oxide particles  
154 around or on the external surface of MSN, however EDS analysis indicated Fe was present  
155 on the template at 1.9 atom % (Table 1, Fig. S1) suggesting the metal was located inside the

156 mesopores, which is consistent with the ca. 10% decrease in pore volume of the material.  
157 Impregnation of the Fe-MSN composite with thiophenol followed by carbonization at 600  
158 °C produced a black material (Fig. 1A, left). In contrast, impregnation of iron-free MSN  
159 with thiophenol and carbonization at 600 °C led to a gray material suggesting low  
160 carbonization efficiency in absence of the metal (Fig. 1A, right). EDS analysis of the  
161 carbonized thiophenol-Fe-MSN composite revealed a homogeneous distribution of C (ca.  
162 50 atom %) and S (ca. 1 atom %) over different areas of the material (Table S1).

163

164 **Scheme 1:** Steps of S-OMC synthesis.



165

166

167 Dissolution of the silica template from the composite in aqueous NaOH yielded a S-  
168 OMC material with well-defined mesopore structure evidenced by TEM imaging,  
169 indicating successful replication of the cylindrical channels of the MSN template (Fig. 1B).  
170 Low angle powder XRD further confirmed the structural relation to the parent MSN  
171 showing a sharp reflection at 0.6 2 $\theta$  degrees associated to the (100) plane of a 2D  
172 hexagonal structure (Fig. 1C). Nitrogen sorption analysis of the S-OMC indicated a type IV  
173 isotherm (Fig. 1d) characteristic of a mesoporous material with narrow pore width  
174 distribution[36] centered at 4.8 nm. Interestingly, the surface area of S-OMC was  
175 significantly larger (ca. 150 %) than the parent MSN (Table 1), likely due to the lower  
176 density of the carbon material. Carbonization at higher temperature (900 °C) led to a drop  
177 in surface area, pore volume, and pore width. Subtracting the pore width from the mesopore  
178 unit cell parameter  $a_0$  ( $a_0 = (2/\sqrt{3})d_{100}$ ) indicated that the higher carbonization temperature  
179 led to thicker pore walls (11.4 nm at 600 °C versus 13.5 nm at 900 °C) and shrinking of the  
180 structure, likely due to cross-linking of poly(phenylene sulfide) via formation of S-  
181 heterocycles during carbonization.[37] Increasing the amount of iron in the synthesis also  
182 led to smaller surface areas, pore volumes and pore widths (Table S2).

183 Table 1: Textural properties and chemical composition of the materials.

	$S_{\text{ABET}}^{\text{a}}$ ( $\text{m}^2/\text{g}$ )	$V_{\text{BJH}}^{\text{b}}$ ( $\text{cm}^3/\text{g}$ )	$w_{\text{BJH}}^{\text{c}}$ (nm)	$\text{C}^{\text{d}}$ (at %)	$\text{O}^{\text{d}}$ (at %)	$\text{Si}^{\text{d}}$ (at %)	$\text{S}^{\text{d}}$ (at %)	$\text{Fe}^{\text{d}}$ (at %)
MSN	400	0.97	7.4	-	$67.0 \pm 1.5$	$33.0 \pm 1.5$	-	-
Fe-MSN	385	0.87	7.3	-	$61.0 \pm 6.5$	$37.1 \pm 6.3$	-	$1.9 \pm 0.3$
S-OMC <sub>600</sub>	596	0.82	4.8	$79.8 \pm 2.0$	$15.9 \pm 1.8$	$2.4 \pm 0.9$	$1.5 \pm 0.7$	$0.5 \pm 0.1$
S-OMC <sub>900</sub>	388	0.39	3.7	$67.2 \pm 1.3$	$27.1 \pm 1.3$	$3.8 \pm 0.1$	$0.5 \pm 0.1$	$1.5 \pm 0.1$

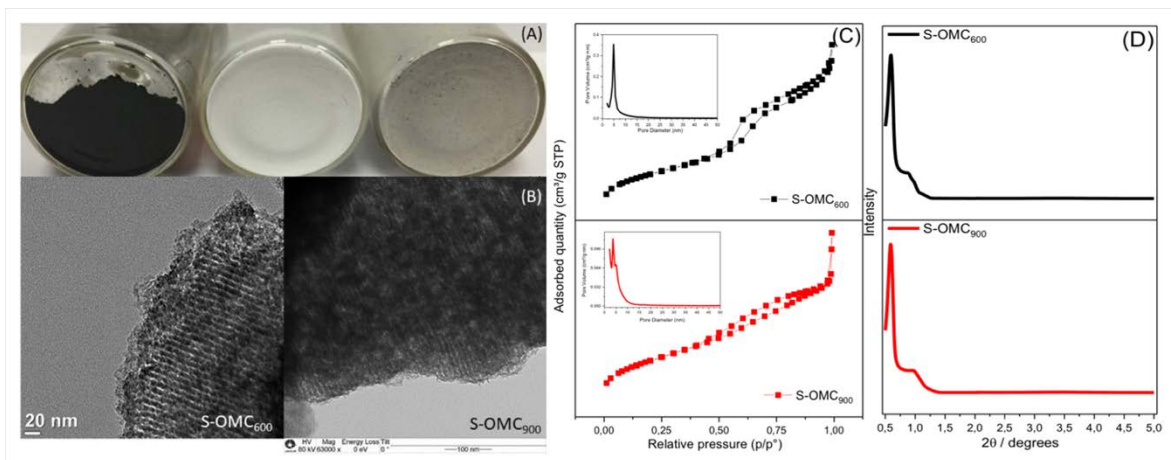
184 <sup>a</sup> Surface area calculated by Brunauer-Emmett-Teller method.

185 <sup>b</sup> Pore volume calculated by Barret-Joyner-Halenda method.

186 <sup>c</sup> Average pore width calculated by Barret-Joyner-Halenda method.

187 <sup>d</sup> Obtained from energy dispersive x-ray spectroscopy.

188  
189



190

195

196 **Fig. 1.** (A) Carbonized thiophenol-MSN composites with (left) and without (right) iron, and  
197 original MSN (middle) for comparison: the gray color of the material without iron suggests  
198 incomplete carbonization as opposed to the black carbonized iron-containing material. (B)  
199 TEM images, (C) N<sub>2</sub> sorption isotherms and pore size distributions (inset), and (D) small-  
200 angle X-ray diffraction patterns of S-OMC carbonized at 600 °C and 900 °C.

201

202 Wide angle XRD analysis of the S-OMC carbonized at 600 °C (S-OMC<sub>600</sub>)  
203 revealed two broad reflections at 23.5 and 44.1 2 $\theta$  degrees that were indexed as d<sub>002</sub> and  
204 d<sub>101</sub> interlayer spacings of carbon planes (Fig. S2A). Both peaks were slightly shifted (26.1  
205 and 42.8) and better defined in the S-OMC carbonized at 900 °C (S-OMC<sub>900</sub>) indicating

206 decreasing d-spacings and increasing degree of graphitization with carbonization  
207 temperature. The  $d_{002}$  interlayer spacing of S-OMC<sub>900</sub> (0.341 nm) is between typical values  
208 for turbostratic (0.344 nm) and graphitic carbon (0.335 nm).[38, 39] Reflections  
209 attributable to iron oxides were only observed at higher iron loadings, and they appear to be  
210 related to magnetite (Fig. S3).[40] In fact, all the OMCs were attracted to magnets.

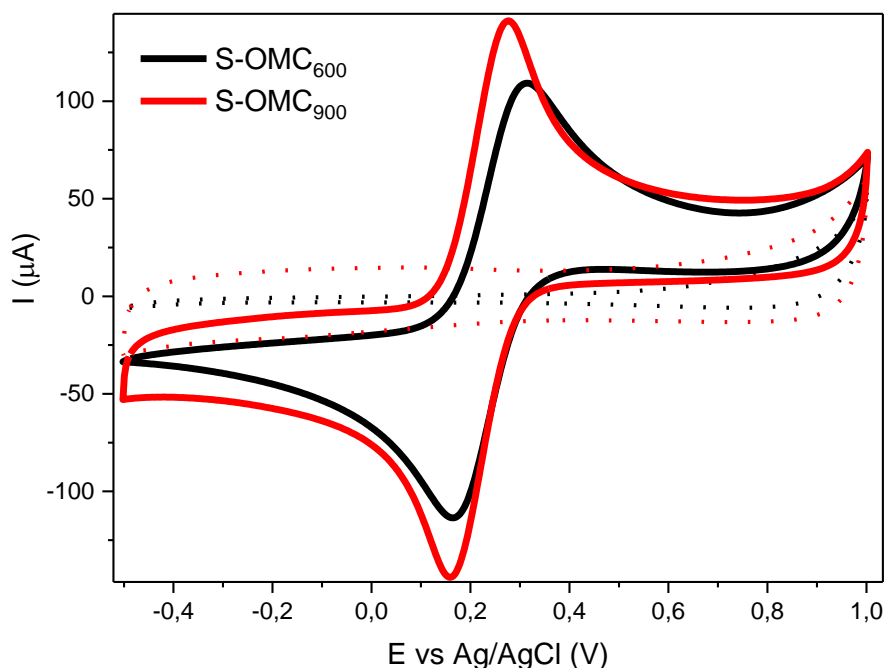
211 Raman spectroscopy of S-OMC<sub>600</sub> and S-OMC<sub>900</sub> showed the characteristic D  
212 ( $1300\text{ cm}^{-1}$ ) and G ( $1590\text{ cm}^{-1}$ ) bands of  $sp^2$  carbon layers (Fig. S2B).[41] Because both  
213 materials show  $I_D/I_G$  ratios larger than 1, the polycyclic aromatic layers should be largely  
214 disordered, yet S-OMC<sub>900</sub> showed a smaller  $I_D/I_G$  ratio (1.36) than S-OMC<sub>600</sub> (1.63),  
215 indicating increasing order (i.e. graphitic character) at higher carbonization temperatures,  
216 which is consistent with the XRD data. Increasing the amount of iron in S-OMC<sub>600</sub> material  
217 also led to lower  $I_D/I_G$  ratios (i.e. improved graphitic character, Fig. S3B,C) further  
218 confirming that iron promotes carbon graphitization. While XRD and Raman data indicate  
219 a more graphitic character of S-OMC<sub>900</sub> than S-OMC<sub>600</sub>, the S content is significantly  
220 lower in the former.

221

### 222 3.2 Electrochemical properties of S-OMC

223 To study the electrochemical behavior of S-OMC the materials were suspended in  
224 DMF, drop casted on clean glassy carbon (GC) electrodes, and dried. Investigation of the  
225 modified electrode/electrolyte interface was carried out by cyclic voltammetry (CV) of  
226  $[\text{Fe}(\text{CN})_6]^{3-/4-}$  (10 mM) from -0.5 to 1 V with KCl electrolyte (0.1 mM) at a  $100\text{ mV s}^{-1}$   
227 scan rate. The cyclic voltammograms obtained using S-OMC<sub>600</sub> and S-OMC<sub>900</sub> modified  
228 glassy carbon (S-OMC/GC) electrodes were acquired in absence and presence of 10 mM  
229  $[\text{Fe}(\text{CN})_6]^{3-/4-}$  (Fig. 2). The  $[\text{Fe}(\text{CN})_6]^{3-/4-}$  redox cycle gave faster electron transfer rates and  
230 higher peak currents on S-OMC<sub>900</sub> ( $\Delta E = 116\text{ mV}$ ,  $132\text{ }\mu\text{A}/-133\text{ }\mu\text{A}$ ) than S-OMC<sub>600</sub> ( $\Delta E =$   
231  $144\text{ mV}$ ,  $107\text{ }\mu\text{A}/-114\text{ }\mu\text{A}$ ) modified GC electrodes. These differences indicate that in spite  
232 of its smaller surface area S-OMC<sub>900</sub> is more electroactive than S-OMC<sub>600</sub>, likely due to  
233 the higher conductivity that results from the increased graphitic character and smaller d-  
234 spacing of the former.

235



236

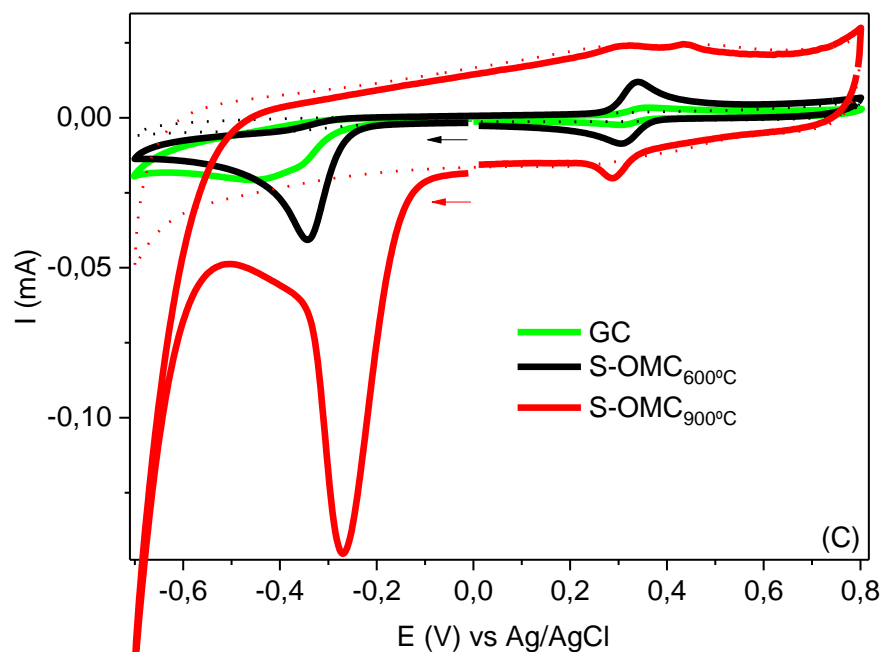
237 **Fig. 2.** Cyclic voltammogram in absence (···) and presence (—) of 10 mM  $[\text{Fe}(\text{CN})_6]^{3-/4-}$  in  
 238 0.1 mM KCl using GC, S-OMC<sub>600</sub>/GC or S-OMC<sub>900</sub>/GC as working electrode.

239

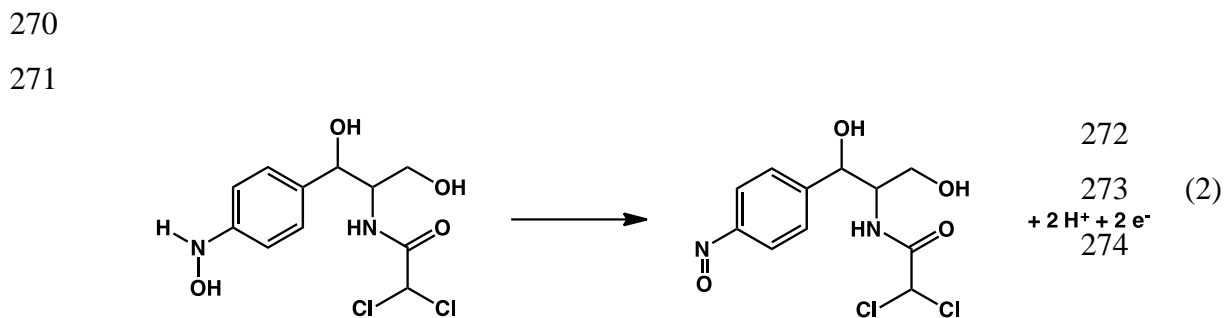
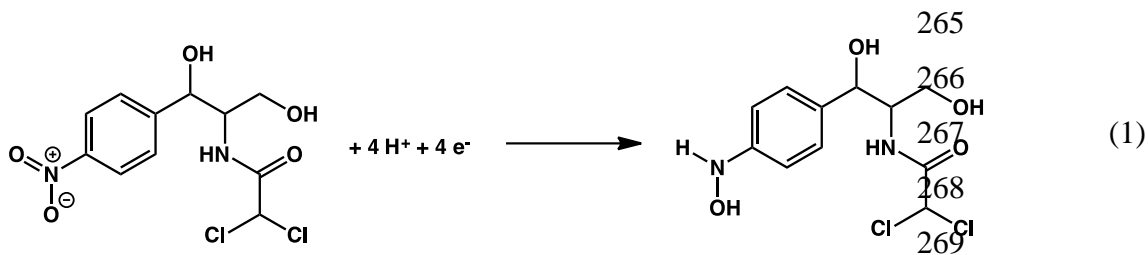
### 240 3.3 Application of S-OMC/GC as chloramphenicol sensors

241 As a proof-of-concept, the two S-OMC/GC electrodes were then used to examine  
 242 the electrochemical behavior of chloramphenicol (CAP) solutions. The cyclic  
 243 voltammograms of CAP (3 mM) on S-OMC<sub>600</sub>/GC and S-OMC<sub>900</sub>/GC in 0.1 M H<sub>2</sub>SO<sub>4</sub>,  
 244 presented well-defined cathodic and anodic peaks attributed to redox transformations of the  
 245 nitro group (Fig. 3).[42] The peak currents obtained with the S-OMC modified electrodes  
 246 were higher and appeared at lower potentials than with the bare GC electrode. The cathodic  
 247 peak appeared at a more negative potential for S-OMC<sub>600</sub>/GC (-343 mV) than S-  
 248 OMC<sub>900</sub>/GC (-270 mV), and was attributed to the irreversible reduction of the nitro group  
 249 to hydroxylamine (Equation 1) based on literature reports.[43, 44] The 73 mV reduction  
 250 underpotential and fourfold peak current enhancement observed for S-OMC<sub>900</sub>/GC relative  
 251 to S-OMC<sub>600</sub>/GC indicated the former is a more efficient electrocatalyst for the reduction  
 252 of the nitro group in CAP than the latter. This behavior is consistent with the results  
 253 obtained from the cyclic voltammetry of  $\text{Fe}(\text{CN})_6^{-4/-3}$ , and can therefore be attributed to the  
 254 increased graphitic character of S-OMC<sub>900</sub>. Interestingly, while the voltammograms of the

255 reaction using S-OMC<sub>600</sub>/GC presented two additional well-defined redox peaks ( $E_R= 307$   
 256 mV;  $E_O= 340$  mV) associated with the reversible interconversion of the hydroxylamine and  
 257 nitroso states (Equation 2),[43, 44] these peaks were significantly less evident when using  
 258 S-OMC<sub>900</sub>/GC, suggesting lower adsorption of the hydroxylamine intermediate onto S-  
 259 OMC<sub>900</sub> than S-OMC<sub>600</sub>.  
 260



261  
 262 **Fig. 3.** Cyclic voltammogram in absence (···) and presence (—) of 3 mM chloramphenicol in  
 263 0.1 M H<sub>2</sub>SO<sub>4</sub> as electrolyte, using GC, S-OMC<sub>600</sub>/GC or S-OMC<sub>900</sub>/GC as working  
 264 electrode.

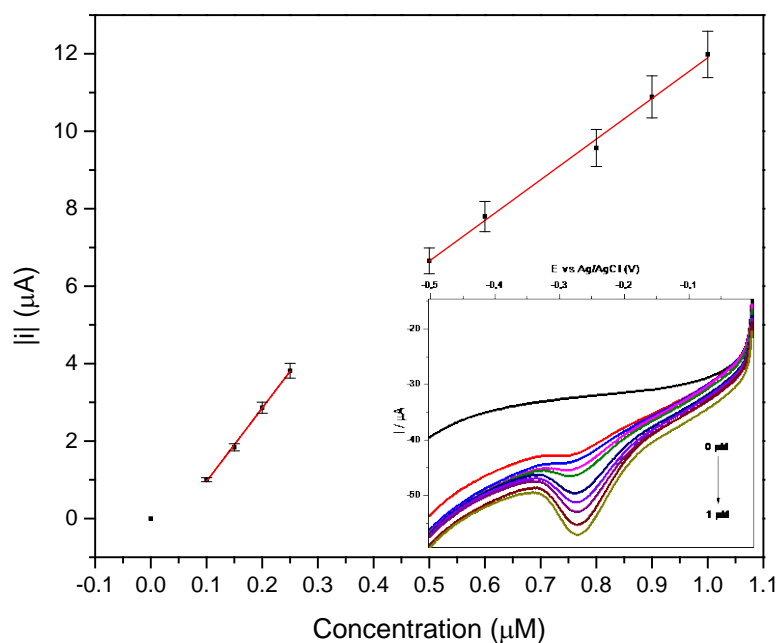


275

276 The effect of scan rate on the cathodic peak current (-270 mV) was investigated to  
277 obtain more insights into the mechanism of the electrochemical reduction of the nitro group  
278 of CAP (Fig. S4). A linear correlation ( $R^2 = 0.999$ ) between the cathodic peak current and  
279 the scan rate was found in the range of 50-400  $\text{mV s}^{-1}$ , suggesting an adsorption-controlled  
280 process.[45] This behavior indicates that the high surface area of the S-OMC materials is  
281 critical to their electrochemical performance. Furthermore, the open mesoporous structure  
282 and large pore volume of S-OMC are key to maximize the accessibility of small molecules  
283 to the electrochemically active surface, and allow loading large amounts of the target  
284 molecules (on the order of  $\text{mmol g}^{-1}$ ). [2, 46] This result suggested that including a pre-  
285 concentration step should increase the capacity of detecting CAP with S-OMC/GC. To  
286 explore this possibility, a linear sweep voltammetry (LSV) of CAP (3 mM in 0.1 M  
287  $\text{H}_2\text{SO}_4$ ) was performed using S-OMC<sub>900</sub>/GC as the work electrode with open circuit pre-  
288 accumulation steps of variable times. The results indicated that the peak current increased  
289 with pre-accumulation time in the range of 0 to 360 s, but no further increase was observed  
290 at longer times (Fig. S5). Therefore, a 360 s pre-accumulation step was applied to all of the  
291 following experiments.

292 The effect of acidity on the behavior of the electrochemical reduction of CAP, was  
293 investigated using phosphate buffered saline (PBS) solutions at pH varying from 1.9 to 10.4  
294 (Fig. S6). The peak potential shifted linearly ( $R^2=0.997$ ) with pH to increasingly negative  
295 values, indicating the participation of  $\text{H}^+$  in the reaction, which is consistent with Equation  
296 (1).[47] Because of the small underpotential in acid electrolytes, a 0.1M  $\text{H}_2\text{SO}_4$  solution  
297 was used to prepare a calibration curve for the quantification of the drug (Fig. 4). The  
298 reduction peak current (-270 mV) increased linearly ( $R^2 = 0.995$ ) with chloramphenicol  
299 concentration (5 to 10  $\mu\text{mol} \cdot \text{L}^{-1}$ ) following the regression equation  $i = 1.4 \times 10^{-6} + 10.5c$  ( $i$   
300 = current in A and  $c$  = concentration in  $\text{mol} \cdot \text{L}^{-1}$ ) with a sensitivity of  $10.5 \text{ A} \cdot \text{L} \cdot \text{mol}^{-1}$ . At  
301 lower concentrations (0.1 to 0.25  $\mu\text{mol} \cdot \text{L}^{-1}$ ), a better sensitivity was obtained ( $18.9 \text{ A} \cdot \text{L} \cdot$   
302  $\text{mol}^{-1}$ ) with good linearity ( $R^2 = 0.997$ ) and regression equation  $i = -9.3 \times 10^{-7} + 18.9c$ . The  
303 limit of detection was calculated as  $7.9 \times 10^{-9} \text{ mol} \cdot \text{L}^{-1}$  ( $\text{LOD} = 3\text{SD}/\text{S}$ ), and the limit of  
304 quantification was  $2.6 \times 10^{-8} \text{ mol} \cdot \text{L}^{-1}$  ( $\text{LOQ} = 10\text{SD}/\text{S}$ ), were SD is the standard deviation  
305 of 10 blank measurements ( $5 \times 10^{-8} \text{ A}$ ) and S is the curve slope ( $18.9 \text{ A} \cdot \text{L} \cdot \text{mol}^{-1}$ ). The

306 obtained values are comparable or better than other electrodes reported in the literature  
307 (Table S2), and highly repeatable, with a 2.3% relative standard deviation (RSD) for ten  
308 consecutive measurements (Fig. S7a). The reproducibility of preparation the S-OMC  
309 modified GC electrodes was estimated by comparing the performances of three freshly  
310 produced electrodes (Fig. S7b). The low RSD (1.8%) obtained for the peak reduction  
311 current measurements demonstrated a highly reproducible manufacturing method.

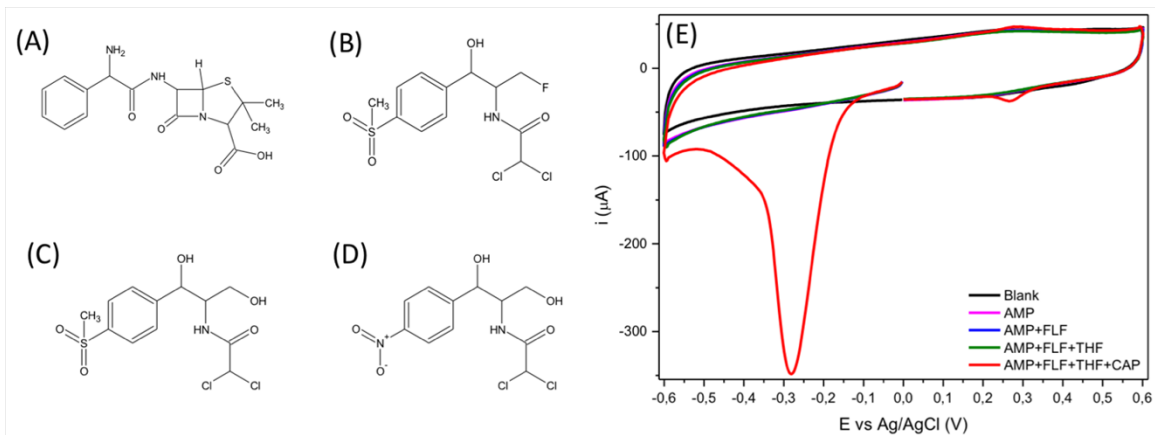


312  
313 **Fig. 4.** Plots of reduction peak current intensity (-270 mV) versus chloramphenicol  
314 concentration. Insert: LSV plots using S-OMC<sub>900</sub>/GC, in  $\text{H}_2\text{SO}_4$  0.1 M in presence of  
315 increasing chloramphenicol concentrations (0.1, 0.15, 0.2, 0.25, 0.5, 0.6, 0.8, 0.9, 1  $\mu\text{mol} \cdot$   
316  $\text{L}^{-1}$ , respectively.)

317  
318 To investigate the selectivity of the sensor, thiamphenicol (TAP) and florfenicol  
319 (FLF), two allowed antibiotics with structures similar to CAP (Fig. 5A-D), were analyzed  
320 as controls. Because ampicillin (AMP) is usually administered in association with CAP, its  
321 potential interference with the detection of the latter was also evaluated. Cyclic  
322 voltammetry experiments of TAP, FLF, AMP (1.5 mM each) and combinations thereof  
323 revealed no peak in the range 0 to -0.6 V, indicating none of the functionalities in these



324 antibiotics was reducible in the same regime as the nitro group in CAP (Fig. 5E). Addition  
325 of CAP (1.5 mM) to a mixture containing all of these antibiotics led to a dramatic increase  
326 in current, demonstrating that the method is selective.



327  
328 **Fig. 5.** Chemical structures of (A) ampicillin (AMP), (B) florfenicol (FLF), (C)  
329 thiamphenicol (THF), and (D) chloramphenicol (CAP); and cyclic voltammetry in absence  
330 and presence of ampicillin, florfenicol, thiamphenicol and chloramphenicol (1.5 mM each)  
331 in H<sub>2</sub>SO<sub>4</sub> 0.1M using S-OMC<sub>900</sub>C/GC as working electrode.

332

333 Finally, the capacity of the S-OMC<sub>900</sub>/GC electrode to detect and quantify CAP in  
334 commercial powdered milk was evaluated. The measurements were carried out using the  
335 standard addition method. For this, commercial powdered milk was dissolved in H<sub>2</sub>SO<sub>4</sub>  
336 0.1M (1 g in 10 mL) and analyzed directly, without any further processing. The LSV of the  
337 reconstituted milk showed no interfering peaks at the detection potential. Upon addition of  
338 CAP in the 50 to 250 μmol L<sup>-1</sup> concentration range, a linear analytical response (R<sup>2</sup> =  
339 0.9996) was obtained with good sensitivity 0.11 A · L · mol<sup>-1</sup> but two orders of magnitude  
340 smaller than the sensitivity in 0.1 M H<sub>2</sub>SO<sub>4</sub>, likely due to matrix interference. The limit of  
341 detection was calculated as 1.9 × 10<sup>-6</sup> mol · L<sup>-1</sup> (LOD = 3SD/S), and the limit of  
342 quantification was 6.3 × 10<sup>-6</sup> mol · L<sup>-1</sup> (LOQ = 10SD/S), where SD is the standard deviation  
343 of 10 blank measurements (7 × 10<sup>-8</sup> A) and S is the curve slope (0.11 A · L · mol<sup>-1</sup>).  
344 Because of this, the method of standard addition is well suited for the application of CV to  
345 the direct determination of CAP in milk, without any sample preparation.

346

347

348

#### 349 **4. Conclusions**

350 Thiophenol was effectively used as a new carbon source for producing S-doped  
351 OMC with SBA-15 type mesoporous silica nanoparticles as a hard template. The process  
352 required iron to facilitate carbon formation, and the graphitic character increased with the  
353 amount of iron employed in the synthesis. Higher carbonization temperatures (900 °C) also  
354 led to increasing graphitic character. The S-OMC<sub>900</sub> material was used to modify a glassy  
355 carbon electrode and presented a small charge transference resistance, high peak current  
356 and smaller underpotential in presence of the redox probe [Fe(CN)<sub>6</sub>]<sup>3-/4-</sup>. The modified  
357 electrode was applied, as proof-of-concept, as a selective CAP sensor. The highly ordered  
358 mesopores and large surface area and pore volume of S-OMC<sub>900</sub>, allowed fast mass  
359 transport of CAP to ensure efficient interaction with the surface of the material. The semi-  
360 graphitic character of the material led to fast electron transfer rates, good conductivity and  
361 less resistive behavior for the electrochemical analysis. The LSV with 360 s pre-  
362 accumulation led to with good sensitivity for CAP detection and nanomolar LOD (7.9 x 10<sup>-9</sup>  
363 mol L<sup>-1</sup>). Also, the proposed methodology allows the direct detection of CAP in powdered  
364 milk, without any sample preparation.

365

#### 366 **Acknowledgments**

367 The authors thank CAPES and CNPq for financial support, INCT/INOMAT – National  
368 Institute of Science, Technology and Innovation in Complex Functional Materials (CNPq-  
369 MCTI/Fapesp) for TEM images. U.C., J.S.M. and I.I.S. acknowledge funding support from  
370 the U.S. Department of Energy, Office of Basic Energy Sciences, Division of Chemical  
371 Sciences, Geosciences, and Biosciences through the Ames Laboratory. The Ames  
372 Laboratory is operated for the U.S. Department of Energy by Iowa State University under  
373 Contract No. DE-AC02-07CH11358.

374

375 **References**

- 376 [1] J.C. Ndamanisha, L.-P. Guo, *Anal. Chim. Acta*, 747 (2012) 19-28.  
377 [2] A. Walcarius, *Trends Anal. Chem.*, 38 (2012) 79-97.  
378 [3] T.-W. Kim, P.-W. Chung, I.I. Slowing, M. Tsunoda, E.S. Yeung, V.S.-Y. Lin, *Nano*  
379 *Lett.*, 8 (2008) 3724-3727.  
380 [4] Y. Zhou, L. Tang, G. Zeng, J. Chen, Y. Cai, Y. Zhang, G. Yang, Y. Liu, C. Zhang, W.  
381 Tang, *Biosens. Bioelectron.*, 61 (2014) 519-525.  
382 [5] F. Li, J. Song, C. Shan, D. Gao, X. Xu, L. Niu, *Biosens. Bioelectron.*, 25 (2010) 1408-  
383 1413.  
384 [6] J.B.Raof, F.Chekin, R.Ojani, S.Barari, M.Anbia, S.Mandegarad, *Anglais*, 16 (2012)  
385 8.  
386 [7] Y. Zhang, X. Bo, A. Nsabimana, C. Luhana, G. Wang, H. Wang, M. Li, L. Guo,  
387 *Biosens. Bioelectron.*, 53 (2014) 250-256.  
388 [8] R. Ryoo, S.H. Joo, M. Kruk, M. Jaroniec, *Adv. Mater.*, 13 (2001) 677-681.  
389 [9] H. Chang, S.H. Joo, C. Pak, *J. Mater. Chem.*, 17 (2007) 3078-3088.  
390 [10] C.H. Kim, D.-K. Lee, T.J. Pinnavaia, *Langmuir*, 20 (2004) 5157-5159.  
391 [11] T.-W. Kim, I.-S. Park, R. Ryoo, *Angew. Chem.*, 115 (2003) 4511-4515.  
392 [12] Y. Xia, R. Mokaya, *Adv. Mater.*, 16 (2004) 1553-1558.  
393 [13] W. Gao, Y. Wan, Y. Dou, D. Zhao, *Adv. Energ. Mater.*, 1 (2011) 115-123.  
394 [14] Z. Wu, Y. Yang, D. Gu, Y. Zhai, D. Feng, Q. Li, B. Tu, P.A. Webley, D.Y. Zhao, *Top.*  
395 *Catal.*, 52 (2009) 12-26.  
396 [15] R. Liu, D. Wu, X. Feng, K. Müllen, *Angew. Chem.*, 122 (2010) 5.  
397 [16] X.Liang, Z.Wen, Y.Liu, H.Zhang, L.Huang, J.Jin, *J.PowerSourc.*,196 (2011)3655-  
398 3658.  
399 [17] H. Wang, C. Zhang, Z. Chen, H.K. Liu, Z. Guo, *Carbon*, 81 (2015) 782-787.  
400 [18] S.-R. Chen, Y.-P. Zhai, G.-L. Xu, Y.-X. Jiang, D.-Y. Zhao, J.-T. Li, L. Huang, S.-G.  
401 Sun, *Electrochim. Acta*, 56 (2011) 9549-9555.  
402 [19] H.I. Lee, S.H. Joo, J.H. Kim, D.J. You, J.M. Kim, J.-N. Park, H. Chang, C. Pak, *J.*  
403 *Mater. Chem.*, 19 (2009) 5934-5939.  
404 [20] K. Kwon, S.-a. Jin, C. Pak, H. Chang, S.H. Joo, H.I. Lee, J.H. Kim, J.M. Kim, *Catal.*  
405 *Today*, 164 (2011) 186-189.  
406 [21] H. Wang, X. Bo, Y. Zhang, L. Guo, *Electrochim. Acta*, 108 (2013) 404-411.  
407 [22] A.P.Terzyk, G.Rychlicki, *Coll.Surf.A: Physicochem. Eng.Aspects*, 163 (2000) 135-  
408 150.  
409 [23] A.P. Terzyk, *Coll. Surf. A: Physicochem. Eng. Aspects*, 177 (2001) 23-45.  
410 [24] M. Seredych, K. László, T.J. Bandoz, *ChemCatChem*, 7 (2015) 2924-2931.  
411 [25] R. Yang, Y. Sun, Z. Yang, J. Wu, in: *Meeting Abstracts, The Electrochemical*  
412 *Society*, 2015, pp. 736-736.  
413 [26] M. Seredych, T.J. Bandoz, *Carbon*, 49 (2011) 1216-1224.  
414 [27] M. Seredych, M. Khine, T.J. Bandoz, *ChemSusChem*, 4 (2011) 139-147.  
415 [28] T.L. Fodey, S.E. George, I.M. Traynor, P. Delahaut, D.G. Kennedy, C.T. Elliott,  
416 S.R.H. Crooks, *J. Immunol. Methods*, 393 (2013) 30-37.  
417 [29] J. Ferguson, A. Baxter, P. Young, G. Kennedy, C. Elliott, S. Weigel, R. Gatermann, H.  
418 Ashwin, S. Stead, M. Sharman, *Anal. Chim. Acta*, 529 (2005) 109-113.  
419 [30] F.T. Fraunfelder, G.C. Bagby, D.J. Kelly, *Am. J. Ophthalmol.*, 93 (1982) 356-360.  
420 [31] K. Krasinski, R. Perkin, J.C. Rutledge, *Clin. Pediat.*, 21 (1982) 571-572.

421 [32] European Commission, RASFF Portal, <https://webgate.ec.europa.eu/rasff->  
422 [window/portal/?event=searchForm&cleanSearch=1](https://webgate.ec.europa.eu/rasff-window/portal/?event=searchForm&cleanSearch=1) (accessed 10/05/2017).  
423  
424 [33] K. Kandel, U. Chaudhary, N.C. Nelson, I.I. Slowing, *ACS Catal.*, 5 (2015) 6719-6723.  
425 [34] W. Li, S. Xie, L. Qian, B. Chang, *Science*, 274 (1996) 1701.  
426 [35] S. Li, G.D. Meitzner, E. Iglesia, *J. Phys. Chem. B*, 105 (2001) 5743-5750.  
427 [36] J. Xu, Z. Luan, H. He, W. Zhou, L. Kevan, *Chem. Mater.*, 10 (1998) 3690-3698.  
428 [37] A. Oya, K. Arai, K. Fujita, *J Mater Sci*, 29 (1994) 4477-4480.  
429 [38] G. Bacon, *Acta Crystallogr.*, 4 (1951) 558-561.  
430 [39] U. Rost, R. Muntean, P. Podleschny, G. Marginean, M. Brodmann, V.A. Şerban, in:  
431 *Solid State Phenomena*, Trans Tech Publ, 2016, pp. 27-32.  
432 [40] X. Dong, H. Chen, W. Zhao, X. Li, J. Shi, *Chem. Mater.*, 19 (2007) 3484-3490.  
433 [41] F. Su, J. Zeng, X. Bao, Y. Yu, J.Y. Lee, X. Zhao, *Chem. Mater.*, 17 (2005) 3960-3967.  
434 [42] S. Chuanuwatanakul, O. Chailapakul, S. Motomizu, *Anal. Sci.*, 24 (2008) 493-498.  
435 [43] J. Borowiec, R. Wang, L. Zhu, J. Zhang, *Electrochim. Acta*, 99 (2013) 138-144.  
436 [44] H. Zhao, Y. Chen, J. Tian, H. Yu, X. Quan, *J. Electrochem. Soc.*, 159 (2012) 6.  
437 [45] D. Zheng, J. Ye, L. Zhou, Y. Zhang, C. Yu, *J. Electroanal. Chem.*, 625 (2009) 82-87.  
438 [46] J. Zang, C.X. Guo, F. Hu, L. Yu, C.M. Li, *Anal. Chim. Acta*, 683 (2011) 187-191.  
439 [47] M. Zhou, L.-P. Guo, Y. Hou, X.-J. Peng, *Electrochim. Acta*, 53 (2008) 4176-4184.  
440 [48] H. Alemu, L. Hlalele, *Bull. Chem. Soc. Ethiopia*, 21 (2007).  
441 [49] T. Alizadeh, M.R. Ganjali, M. Zare, P. Norouzi, *Food Chem.*, 130 (2012) 1108-1114.  
442 [50] X. Zhang, Y.-C. Zhang, J.-W. Zhang, *Talanta*, 161 (2016) 567-573.  
443 [51] L. Agüí, A. Guzmán, P. Yáñez-Sedeño, J.M. Pingarrón, *Anal. Chim. Acta*, 461 (2002)  
444 65-73.  
445 [52] M.L. Mena, L. Agüí, P. Martínez-Ruiz, P. Yáñez-Sedeño, A.J. Reviejo, J.M.  
446 Pingarrón, *Anal. Bioanal. Chem.*, 376 (2003) 18-25.  
447 [53] F.-Y. Kong, T.-T. Chen, J.-Y. Wang, H.-L. Fang, D.-H. Fan, W. Wang, *Sens.*  
448 *Actuators B Chem.*, 225 (2016) 298-304.  
449 [54] M. Zhu, Y. Zhang, J. Ye, H. Du, *Int. J. Electrochem. Sci.*, 10 (2015) 8263-8275.  
450

451 Supplementary material

452 **Development of a semigraphitic sulfur-doped ordered**  
453 **mesoporous carbon material for electroanalytical applications**

454 Jaqueline R Maluta<sup>A</sup>, Sergio A S Machado<sup>A</sup>, Umesh Chaudhary<sup>B</sup>, J. Sebastián Manzano<sup>B</sup>,  
455 Lauro T Kubota<sup>C</sup>, Igor I. Slowing<sup>B,\*</sup>

456

457 <sup>A</sup> São Carlos Institute of Chemistry, University of São Paulo, CP 380, CEP 13566-590, São  
458 Carlos, São Paulo, Brazil

459 <sup>B</sup> Ames Laboratory and Department of Chemistry, Iowa State University, Ames, Iowa  
460 50011, United States

461 <sup>C</sup> Department of Analytical Chemistry, Institute of Chemistry – UNICAMP, P.O. Box  
462 6154, 13084-971, Campinas, SP, Brazil

463

464

465

466

467

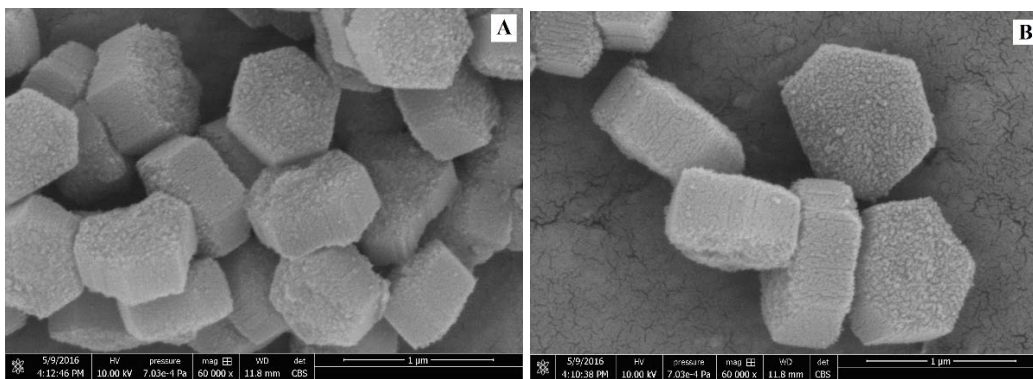
468

469

470

471

472



473

474 **Fig. S1.** SEM-FEG-DBS images of the (A) SBA-15 type MSN and (B) Fe-MSN  
 475 composite.

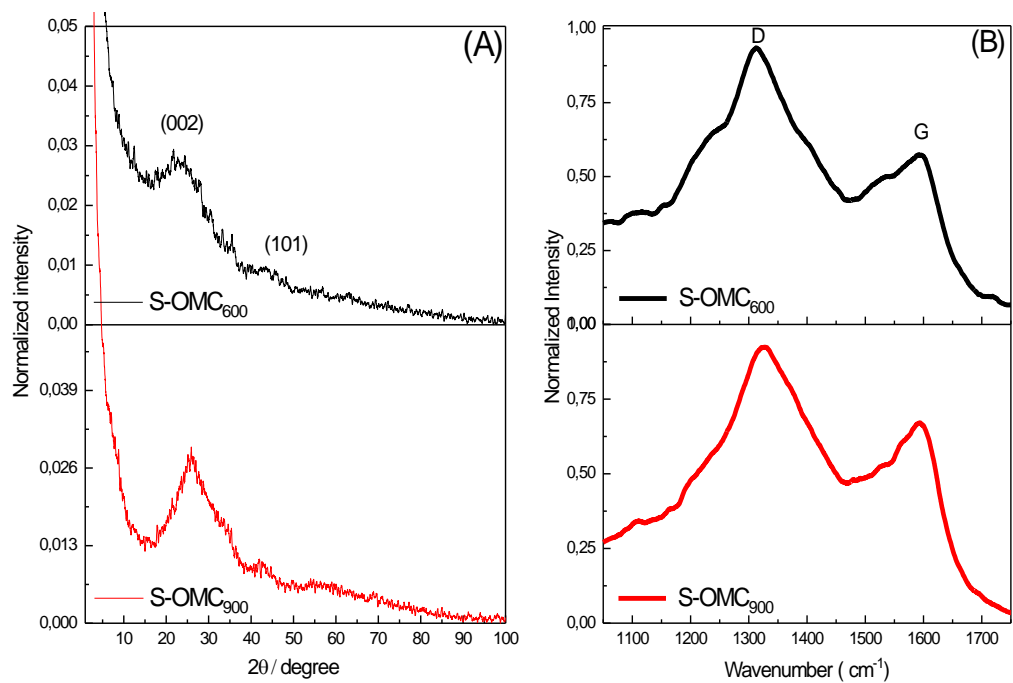
476

477 **Table S1.** Chemical composition by EDS of the thiophenol-Fe-MSN material carbonized at  
 478 600 °C.

	Area 1	Area 2
C	49.01	51.03
O	37.68	36.72
Si	11.55	10.48
S	1.05	1.12
Fe	0.71	0.64
C/Si	4.3	4.9

479

480

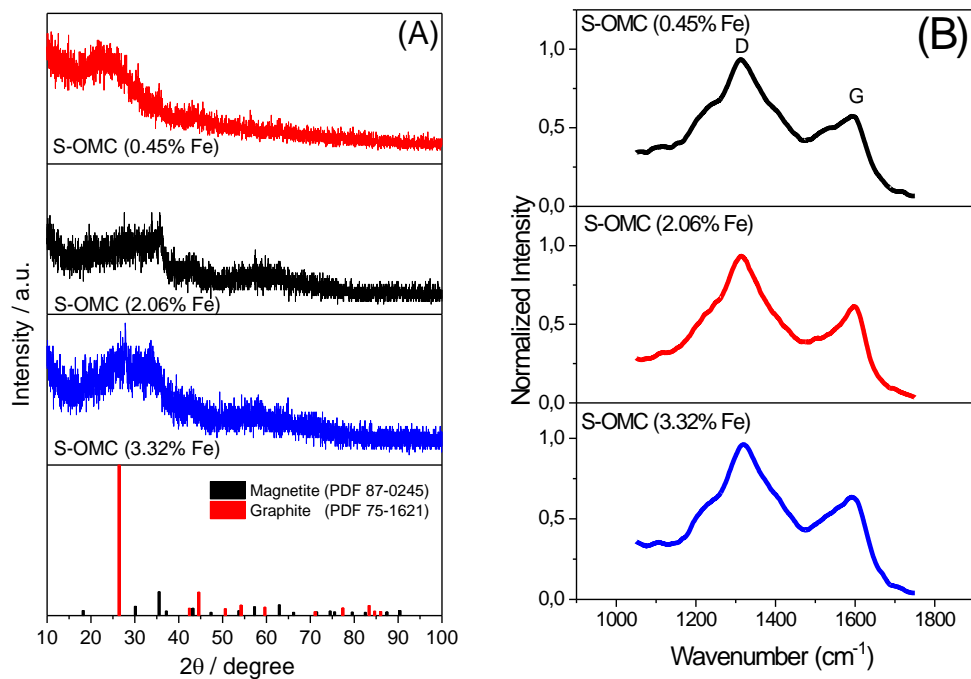


481

482 **Fig. S2.** (A) Wide-angle X-ray diffraction and (B) Raman of S-OMC<sub>600</sub> and OMC<sub>900</sub>.

483

484



485

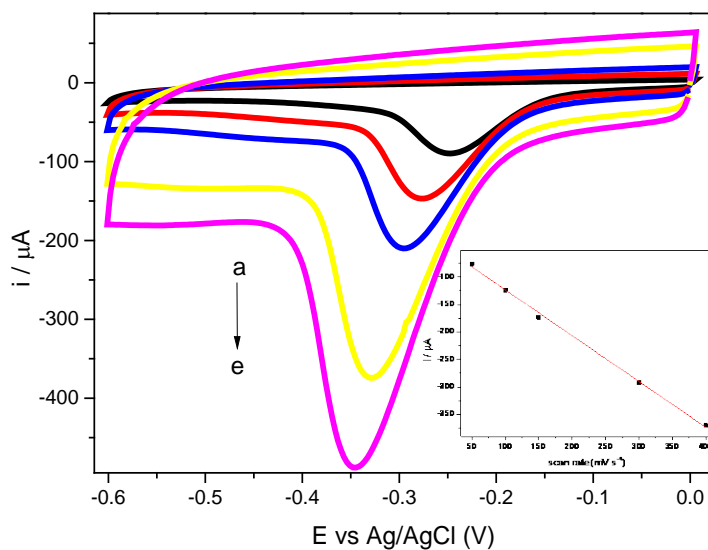
486

487 **Fig. S3.** Wide-angle X-ray diffraction (A) and Raman (B) of materials synthesized with

488 varying iron content. (C) Relation between the I<sub>D</sub>/I<sub>G</sub> and the iron quantity.

489



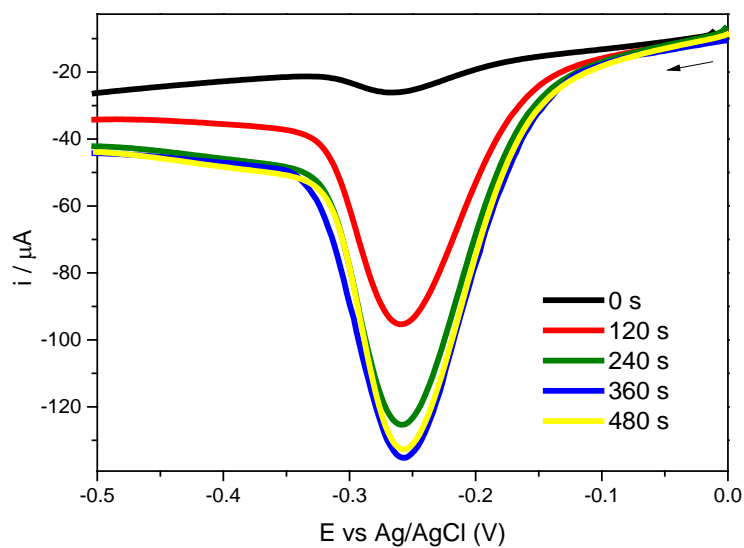


490

491 **Fig. S4.** Cyclic voltammetry of chloramphenicol using or S-OMC<sub>900</sub>/GC as work electrode  
 492 in 0.1 M H<sub>2</sub>SO<sub>4</sub>. From a to e, scan rate of 50, 100, 150, 300, 400 mV s<sup>-1</sup>, respectively.

493 Insets: Plots of  $i_{pc}$  versus scan rate.

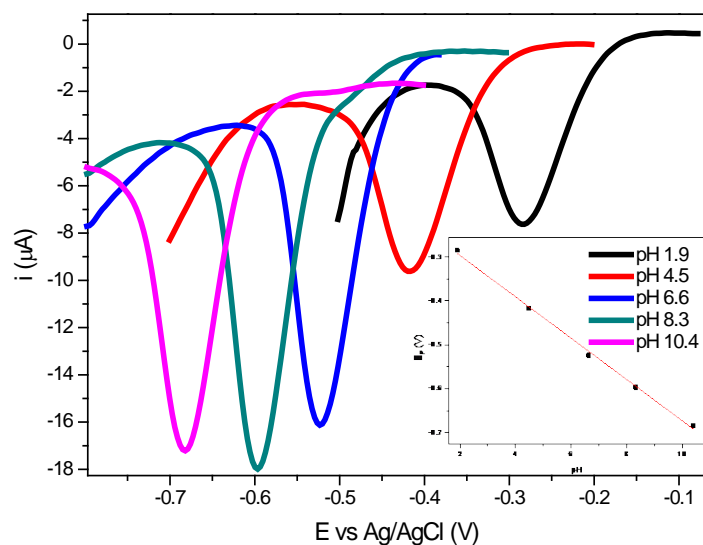
494



495

496 **Fig. S5.** LSV in H<sub>2</sub>SO<sub>4</sub> 0.1 M in presence of chloramphenicol with pre-concentration times  
 497 of 0, 120, 240, 360 or 480 s under stirring.

498



499

500 **Fig. S6.** LSV of chloramphenicol record with S-OMC<sub>900</sub>/GC modified electrode in PBS at  
 501 pH varying from 1.9 to 10.4. Inset: relation between the electrolyte pH and the peak  
 502 potential.

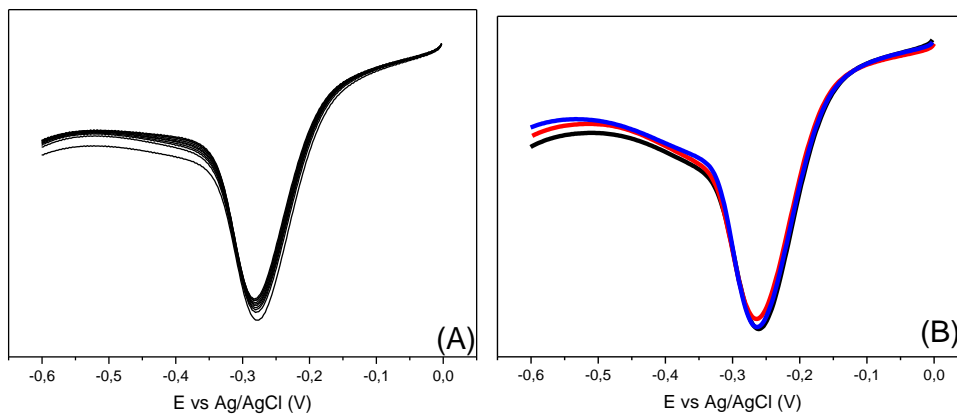
503

504 **Table S2.** Electrochemical determination of chloramphenicol using different electrodes.

	Technique	Detection limit (mol L <sup>-1</sup> )	Electrode
[43]	LSV (540 s)	5.9 x 10 <sup>-7</sup>	N-graphene / AuNP
[44]	DPV	7.4 x 10 <sup>-8</sup>	MIP/MWNT-AuNP
[48]	SWV	6 x 10 <sup>-9</sup>	Pretreated GC
[49]	DPV	2 x 10 <sup>-9</sup>	MIP-Carbon Paste
[50]	DPV	1.5 x 10 <sup>-5</sup>	3D-rGO
[51]	SWV	4.7 x 10 <sup>-8</sup>	Activated carbon fiber
[52]	SWV	4.7 x 10 <sup>-8</sup>	Carbon fiber
[53]	LSV (210 s)	2 x 10 <sup>-8</sup>	TiN-rGO
[54]	LSV (240 s)	8.5 x 10 <sup>-9</sup>	Nafion/OMC
This work	LSV (360 s)	7.9 x 10 <sup>-9</sup>	S-OMC

505 \* LSV = linear sweep voltammetry; AuNP = Gold nanoparticle; DPV = differential pulse  
506 voltammetry; MIP = molecularly imprinted polymer; SWV = square wave voltammetry;  
507 MWCNT = multiwall carbon nanotube; TiN-rGO = Tetrapods-like titanium nitride-  
508 reduced graphene oxide.

509



510

511 **Fig. S7.** Linear voltammetry in 0.1M H<sub>2</sub>SO<sub>4</sub> in presence of 1.5 mM of chloramphenicol  
512 using (A) the same electrode ten times and (B) three freshly produced electrodes S-  
513 OMC<sub>900</sub>.